Human Molecular Genetics, 2009, Vol. 18, No. 12 **2149–2165**
doi:10.1093/hmg/ddp148
Advance Access published on March 25, 2009

Loss-of-function mutations in *ATP6V0A2* impair vesicular trafficking, tropoelastin secretion and cell survival

Vishwanathan Hucthagowder[1,†], Eva Morava[4,†], Uwe Kornak[6,7,†,‡], Dirk J. Lefeber[5], Björn Fischer[6], Aikaterini Dimopoulou[6], Annika Aldinger[1], Jiwon Choi[8], Elaine C. Davis[8], Dianne N. Abuelo[9], Maciej Adamowicz[10], Jumana Al-Aama[11], Lina Basel-Vanagaite[12,13,‡], Bridget Fernandez[14], Marie T. Greally[15,‡], Gabriele Gillessen-Kaesbach[16], Hulya Kayserili[17,‡], Emmanuelle Lemyre[18], Mustafa Tekin[19], Seval Türkmen[6], Beyhan Tuysuz[20], Berrin Yüksel-Konuk[19], Stefan Mundlos[6,7,‡], Lionel Van Maldergem[21,‡], Ron A. Wevers[5] and Zsolt Urban[1,2,3,*]

[1]Department of Pediatrics, [2]Department of Genetics, [3]Department of Medicine, Washington University School of Medicine, 660 South Euclid Avenue, Campus Box 8208, St Louis, MO 63110, USA, [4]Department of Pediatrics, [5]Laboratory of Pediatrics and Neurology, Radboud University Nijmegen Medical Centre, Nijmegen 6525GA, The Netherlands, [6]Institute for Medical Genetics, Charité Universitätsmedizin, Berlin 13353, Germany, [7]Development and Disease Research Group, Max Planck Institute for Molecular Genetics, Berlin 14195, Germany, [8]Department of Anatomy and Cell Biology, McGill University, Montreal, Canada H3A 2B2, [9]Department of Pediatrics, Rhode Island Hospital, Hasbro Children's Hospital and Brown University School of Medicine, Providence, RI 02903, USA, [10]Department of Biochemistry and Experimental Medicine, The Children's Memorial Health Institute, Warsaw 04730, Poland, [11]Princess Al Jawhara Center of Excellence in the Research of Hereditary Disorders, King Abdulaziz University, Jeddah 21486, Saudi Arabia, [12]Schneider Children's Medical Center of Israel and Raphael Recanati Genetics Institute, Rabin Medical Center, Beilinson Campus, Petah Tikva 49202, Israel, [13]Sackler Faculty of Medicine, Tel Aviv University, Ramat Aviv 69978, Israel, [14]Medical Genetics Program, Eastern Health, St John's, Canada A1B 3V6, [15]The National Centre for Medical Genetics, Our Lady's Children's Hospital, Crumlin, Dublin 12, Ireland, [16]Institut für Humangenetik, Universität zu Lübeck, Lübeck 23538, Germany, [17]Istanbul Medical Faculty, Medical Genetics Department, Istanbul University, Istanbul 34390, Turkey, [18]Service de Génétique Médicale, CHU-Ste-Justine, Montreal, Quebec, Canada, [19]Department of Pediatrics, Ankara University School of Medicine, Ankara 06100, Turkey, [20]Department of Pediatric Genetics, Cerrahpasa Medical School, Istanbul University, Istanbul 34452, Turkey and [21]Centre de Génétique Humaine, Centre Hospitalier Universitaire du Sart-Tilman, Université de Liège, Liège 4000, Belgium

Received December 5, 2008; Revised February 27, 2009; Accepted March 23, 2009

Autosomal recessive cutis laxa type 2 (ARCL2), a syndrome of growth and developmental delay and redundant, inelastic skin, is caused by mutations in the a2 subunit of the vesicular ATPase H^+-pump (ATP6V0A2). The goal of this study was to define the disease mechanisms that lead to connective tissue lesions in ARCL2. In a new cohort of 17 patients, DNA sequencing of *ATP6V0A2* detected either homozygous or compound heterozygous mutations. Considerable allelic and phenotypic heterogeneity was observed, with a missense mutation of a moderately conserved residue p.P87L leading to unusually mild disease. Abnormal N- and/or mucin type O-glycosylation was observed in all patients tested. Premature stop codon mutations led to decreased *ATP6V0A2* mRNA levels by destabilizing the mutant mRNA via the nonsense-mediated decay pathway. Loss of *ATP6V0A2* either by siRNA knockdown or in ARCL2 cells resulted in

*To whom correspondence should be addressed. Tel: +1 3142862973; Fax: +1 3142862893; Email: urban_z@kids.wustl.edu
†The authors wish it to be known that, in their opinion, the first three authors should be regarded as joint First Authors.
‡These authors belong to the ARCL Debré-type study group.

distended Golgi cisternae, accumulation of abnormal lysosomes and multivesicular bodies. Immunostaining of ARCL2 cells showed the accumulation of tropoelastin (TE) in the Golgi and in large, abnormal intracellular and extracellular aggregates. Pulse–chase studies confirmed impaired secretion and increased intracellular retention of TE, and insoluble elastin assays showed significantly reduced extracellular deposition of mature elastin. Fibrillin-1 microfibril assembly and secreted lysyl oxidase activity were normal in ARCL2 cells. TUNEL staining demonstrated increased rates of apoptosis in ARCL2 cell cultures. We conclude that loss-of-function mutations in *ATP6V0A2* lead to TE aggregation in the Golgi, impaired clearance of TE aggregates and increased apoptosis of elastogenic cells.

INTRODUCTION

Cutis laxa is an acquired or inherited skin disease characterized by pendulous, redundant and inelastic skin. Inherited forms of this disease show remarkable locus heterogeneity. All cutis laxa syndromes described to date are associated with elastic fiber abnormalities. X-linked cutis laxa or occipital horn syndrome (MIM 304150) is caused by mutations in the *ATP7A* Cu^{2+} transporter gene (1). Cu^{2+} is an essential cofactor of lysyl oxidases (LOXs), a family of enzymes necessary for cross-linking fibrillar collagens and elastin. Autosomal dominant cutis laxa (MIM 123700) is caused by mutations in the elastin gene (*ELN*) (2–7), encoding the main structural component of elastic fibers. Autosomal recessive cutis laxa type 1 (MIM 219100), characterized by severe developmental emphysema and tortuosity, aneurysms or obstructive disease of the main systemic and pulmonary arteries has been shown to be caused by a mutation in *FBLN5* (8,9) or *EFEMP2* (10,11), encoding the elastic fiber proteins fibulin-5 and fibulin-4 (also known as epidermal growth factor-containing fibulin-like extracellular matrix protein 2), respectively.

Autosomal recessive cutis laxa type 2 (ARCL2), also known as Debré-type cutis laxa (MIM 219200), is associated with growth and developmental delay, facial dysmorphia, delayed closure of the fontanelle, structural brain abnormalities, seizures, frequent mental impairment and combined disorder of N- and O-linked glycosylation (12). Thus, ARCL2 can also be considered as a congenital disorder of glycosylation (CDG), member of a growing group of inherited diseases characterized by impaired attachment of sugars to proteins in the secretory pathway (13). CDGs are caused by mutations in glycosyl transferases, sugar transporters and subunits of the conserved oligomeric Golgi (COG) involved in membrane trafficking (14–16). Among CDGs, *COG7* mutations can result in wrinkly skin (16), but these patients can be differentiated from ARCL2 based on clinical and biochemical criteria (17).

ARCL2 shares many features with wrinkly skin syndrome [WSS (MIM 278250)]. A whole genome linkage and positional cloning study led to the discovery of the gene for both ARCL2 and WSS (18). The causative gene, *ATP6V0A2*, encodes the a2 subunit of the vesicular H^+-pump. The goals of this study were to better define the phenotypes and genotypes associated with ARCL2 and to uncover the mechanisms leading to elastic fiber abnormalities in this disease.

RESULTS

Clinical and biochemical findings

The clinical features of the 17 patients included in this study are summarized in Table 1. Most patients were singletons. Familial cases included a sibling pair represented by Patients 7 and 8; Patients 11, 14 and 16 were from families with 2, 2 and 3 affected sibs, respectively. Detailed clinical description of Patients 1–6, 7, 8 and 16 has been published earlier (12,19). All children were born at term, except for Patient 6 (born at 35 weeks of gestation). No abnormalities were observed during the pregnancies, except for oligohydramnios in Patient 4. All patients, except for Patients 2 and 4, had normal growth parameters at birth. Congenital microcephaly was observed in Patients 2, 3, 4 and 6. The most frequently observed clinical lesions were the following: characteristic facial features (Fig. 1A–H), neonatal presence of cutis laxa or wrinkly skin (Fig. 1C, E–G, I and J), large anterior fontanelle with delayed closure, joint laxity, eye abnormalities (Fig. 1B), microcephaly (Fig. 1H), developmental delay, intellectual disability and partial pachygyria. Ophthalmologic evaluation showed strabismus in 13 patients (Patients 2–5, 7–10 and 14–16). Myopia (< -5 diopters) was detected in Patients 1 and 5 and hyperopia in Patient 6. Brain developmental anomalies included lesions of variable severity in nine children; multicystic frontal lesions, bilateral frontotemporal pachygyria/polymicrogyria, white matter anomalies, delayed myelinization and cerebellar hypoplasia.

Most patients had at least 5 of the 10 common lesions associated with ARCL2, also including growth delay and hernias. Besides the sporadic occurrence of congenital joint anomalies (bilateral hip dislocation in Patient 4) and seizures (Patient 5), other less frequent anomalies of clinical importance were observed including cardiovascular (coarctation of the aorta with bicuspid aortic valve and atrioventricular septal defect in Patients 6, 8 and 9), urogenital (vesico-urinary reflux and ureter dilatation in Patients 4, 9 and 10), hematologic (prolonged activated partial thromboplastin time and decreased factor XI levels in Patients 3 and 14) and hepatic function (elevated alanine aminotransferase and aspartate aminotransferase levels in Patients 1 and 2) abnormalities.

Isoelectric focusing of serum proteins indicated an isolated O-glycosylation abnormality in Patients 2 and 4 at a very young age (<6 months, Fig. 1K and L, lane P4a), whereas repeat samples showed a combined N + O-glycosylation disorder in both cases (Fig. 1K and L, lane P4b). Most patients tested showed abnormal N- and O-linked glycosylation,

Table 1. Clinical characteristics of ARCL2 patients

Clinical features	P 1	P 2	P 3	P 4	P 5	P 6	P 7	P 8	P 9	P 10	P 11	P 12	P 13	P 14	P 15	P 16	P 17	Frequency
Cutis laxa	+	+	+	+	+	+	±[a]	±[a]	+	+	+[a]	+[a]	+	+	+	+	+	1.00
Large fontanelles or delayed closure	+	+	+	+	+	+	+	+	+	+	+	+	NA	+	+	+	+	1.00
Joint laxity	+	+	+	+	+	+	−	+	+	+	+	−	−	+	+	+	+	0.82
Microcephaly	−	+	++	++	+	+	++	++	+	−	+	+	−	+	+	++	+	0.82
Eye anomalies	+	+	+	+	+	+	+	+	+	+	−	−	−	+	+	+	−	0.76
Developmental delay, MR	+	+	++	−	−	−	+	+	++	+	−	++	−	+	+	++	++	0.71
Partial pachygyria	−	−	+	−	−	+	+	+	±	+	−	NA	NA	+	+	+	−	0.57
SGA or delayed growth	−	+	+	+	+	+	−	−	−	−	+	+	−	−	−	−	+	0.47
Hernias	−	−	−	−	−	−	+[b]	−	+[b]	NA	+[c]	+[c]	+[b]	+[b]	+[b]	−	−	0.44
Congenital cardiac anomalies	−	−	−	−	−	+	−	+	+	−	−	−	−	−	−	−	−	0.18
Congenital urogenital anomalies	−	−	−	+	−	−	−	−	+	+	−	−	−	−	−	−	−	0.18
Coagulation anomalies	−	−	+	−	−	−	−	−	−	−	−[d]	−	NA	+	−	NA	−	0.13
Liver function anomalies	+	+	−	−	−	−	−	−	−	−	−	−	NA	−	−	−	−	0.13
Congenital joint anomalies	−	−	−	+	−	−	−	−	−	−	−	−	−	−	−	−	+	0.12
Seizures	−	−	−	−	+	−	−	−	−	−	−	−	−	−	−	−	−	0.06
Clinical score	0.35	0.41	0.65	0.53	0.41	0.47	0.47	0.53	0.62	0.44	0.35	0.44	0.15	0.53	0.47	0.56	0.47	

Clinical score. The presence of each symptom is equal to score 1 (+). A double score was allowed for microcephaly and for developmental delay/MR depending on the quantitative severity measures: severe microcephaly (++; OFC ≤ -4SD), moderate microcephaly (+; -4 SD $<$ OFC ≤ -2SD), mild developmental delay or metal retardation (MR, ++; $50 <$ IQ ≤ 70), borderline MR (score 1; $70 <$ IQ ≤ 80) and no MR (−, $80 <$ IQ). For each patient, a clinical score was calculated by dividing the sum of scores by the maximal total score. P, patient; SGA, small for gestational age; NA, not available; [a]Wrinkly skin; [b]Inguinal hernia; [c]Umbilical hernia; [d]Sickle cell anemia.

whereas some (Patients 10, 12 and 13) showed an isolated N-glycosylation defect (Table 2). The types of both N- and O-glycosylation profiles were consistent in all patients: a typical disialotransferrin isofocusing profile with increased disialo- and trisialotransferrin fractions (Fig. 1K, lane P4b) was combined with an $ApoCIII_1$ profile with increased levels of mono-sialylated $ApoCIII_1$ and decreased di-sialylated $ApoCIII_2$ isoforms (Fig. 1L, lane P4b).

ATP6V0A2 mutations in ARCL2

To identify the molecular basis of ARCL2 in these patients, we searched the *ATP6V0A2* gene for mutations by direct sequencing. Either homozygous or compound heterozygous mutations were identified in 17 patients yielding a total of 18 different mutations (Table 3 and Fig. 2). A high level of allelic heterogeneity was observed including nonsense ($n = 4$), frameshift ($n = 7$), splice site ($n = 2$), exon deletion ($n = 1$) and missense ($n = 4$) mutations distributed evenly across the gene with no evidence of clustering. In the present study, homozygous deletion of exon 16 was found in four independently identified individuals, three from Turkey and one from Iran (Fig. 2B). Mutation p.Q765X, found in two patients in this study, has been previously reported in a different patient (18). All other mutations reported here were unique. To confirm the mutations, parental samples were genotyped if available. Both parents of Patients 5, 7 and 8, 14 and 16 were heterozygous for one mutation each.

The majority of the mutations were expected to severely disrupt the function of ATP6V0A2 either by introducing premature termination codons (PTCs) and altering splicing or by deleting important domains. Four missense mutations were found. Patient 13 was compound heterozygous for missense mutation p.P87L and frameshift mutation p.S27fsX54. The P87 residue showed conservation in mammals but not in other vertebrates (Fig. 3A). Consistent with p.P87L being a hypomorphic mutation, Patient 13 showed very mild manifestations limited to cutis laxa and inguinal hernia, and a correspondingly low clinical severity score of 0.15 (Table 1).

Patient 1 carried two missense mutations, both in a homozygous state. Mutation p.P405L was located adjacent to the first transmembrane (TM) helix and p.R510I in the second lumenal loop region (Fig. 2A). Although P405 was conserved in all vertebrates, R510 was not (Fig. 3A), suggesting that P405L was the likely disease allele. Patients 7 and 8 were homozygous for p.P792R. Residue P792 is located in the 9th TM helix (Fig. 2A) and is highly conserved in vertebrates (Fig. 3). The clinical manifestations of Patient 1 were moderately severe (clinical score = 0.35) (Table 1). Patients 7 and 8 were severely affected (clinical scores = 0.47 and 0.53) (Table 1). Although the mean clinical score of patients with at least one missense mutation was less compared with those with only premature termination mutations or homozygous exon 16 deletion, this difference was not significant statistically (Fig. 3B). High frequency of proline substitution mutations in ARCL2 suggests that prolines located in the proximity or within the TM helices are essential for ATP6V0A2 function. Indeed, recent biophysical studies have demonstrated that prolines are essential for the thermodynamic and structural stability of TM helices (20).

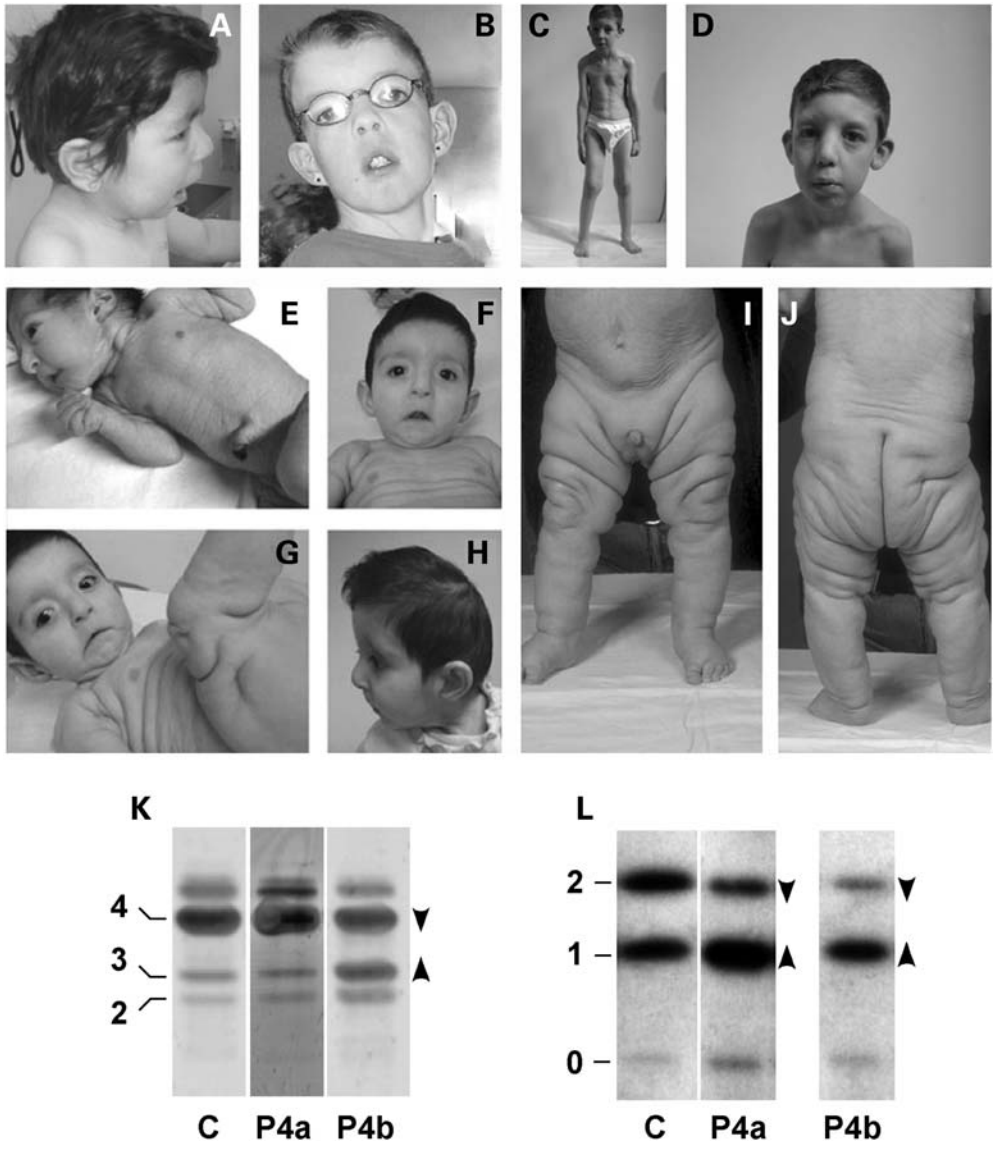

Figure 1. Clinical characteristics and glycosylation abnormalities in ARCL2. Characteristic facial features include short nose (**A, B** and **H**), broad nasal bridge (B, **D** and **G**), long philtrum (A, B and D), and down-slanting corners of the mouth (B, **F** and G) and of the palpebral fissures (B, D, F and G). Cutis laxa of the abdominal region with fine wrinkled skin (**C, E** and **I**). Cutis laxa with unequal fat distribution (I and **J**). (**K**) N-glycosylation by isofocusing of transferrin was similar to control (C) in Patient 4 at 2 months (P4a), but was abnormal at >1 year (P4b) showing reduced tetasialo- (4, arrowhead down) and increased trisialo- (3, arrowhead up) and disialotransferrin (2). (**L**) Mucin type O-glycosylation by isofocusing of apolipoprotein CIII showed abnormally decreased $CIII_2$ isoform and increased $CIII_1$ isoform in Patient 4 both at 2 months (P4a) and at >1 year (P4b).

ATP6V0A2 mutations cause reduced mRNA expression

To investigate the impact of ARCL2 mutations on the biosynthesis of ATPV0A2, we used skin fibroblasts from Patient 1 (homozygous for missense mutations p.P405L and p.R501I), Patient 5 (compound heterozygote for mutations p.R133fsX135 and p.W822X), Patient 9 (homozygous for the exon 16 deletion), Patient 13 (compound heterozygote for missense mutation p.P87L and frameshift p.S27fsX54) and a patient who was homozygous for mutation p.Q765X, like Patient 14. Real-time polymerase chain reaction (PCR) analysis showed that patients with at least one mutation predicted to introduce a PTC had significantly reduced steady state *ATP6V0A2* mRNA levels (Fig. 4A). In contrast, abundance of *ATP6V0A2* mRNA with missense mutations was not significantly different from control. Upon incubation with cycloheximide (CHX), which blocks nonsense-mediated decay, the expression of mutations p.R133fsX135 and p.Q765X increased (Fig. 4B and D). Interestingly, mutation S27fsX54 was not expressed at the mRNA level (Fig. 4C), even after treatment with CHX, suggesting that this mutation interferes with either transcription or RNA stability through a different mechanism.

Abnormal Golgi apparatus and vesicles in ARCL2

We investigated the consequences of ATP6V0A2 deficiency by siRNA knockdown experiments in HeLa cells. The loss of the a2

Table 2. Glycosylation defects in ARCL2 patients

Clinical score Max: 1.00	Patient	Age (year)	Transferrin Disialo (%)	Trisialo (%)	$ApoCIII_1$ (%)	$ApoCIII_2$ (%)
0.35	1	1–18	**16**	**32**	**80**	**14**
0.41	2	0–1	**11**	**30**	**82**	**15**
0.65	3	1–18	**11**	**29**	**89**	**7**
0.53	4	1–18	6	**22**	**89**	**8**
0.41	5	>18	**12**	**28**	**91**	**7**
0.47	6	1–18	**17**	**30**	**77**	**20**
0.47	7	1–18	7	**25**	**77**	**14**
0.53	8	1–18	8	**31**	**81**	**12**
0.62	9	1–18	**10**	**26**	**84**	**9**
0.44	10	1–18	**11**	**28**	**66**	**26**
0.44	12	1–18	**10**	**25**	60	34
0.15	13	>18	**13**	**27**	**70**	27
		Ref: all ages	2.5–9.8	3.4–13.7		
		0–1 year			34–59	40–62
		1–18 years			33–67	27–60
		>18 years			43–69	23–50

Data outside of the reference range are shown in bold type.

Table 3. *ATP6V0A2* mutations in ARCL2

Patient	Origin	Exon	Status	Genomic	cDNA	Protein
1	Belgium	11	hom	g.31908C>T	c.1214C>T	p.P405L
		13	hom	g.32579G>T	c.1529G>T	p.R510I
2	Iran[a]	16	hom	g.38642–39025del388 bp	c.1936_2055del	p.E646_685del
3	Poland	16	het	g.38872T>A	c.2015T>A	p.L672X
		2	het	g.6318delG	c.130delG	p.N43fsX55
4	Turkey[a]	16	hom	g.38642–39025del388 bp	c.1936_2055del	p.E646_685del
5	USA	4	het	g.12439_12440insCATGCTGA	c.397_398insCATGCTGA	p.R133fsX135
		i19	het	g.45608A>G	c.2466_2470delGGTAG	p.W822X
6	French	11	het	g.31992delA	c.1298delA	p.E432fsX444
	Canadian	12	het	g.32468G>A	c.1514+1G>A	NA
7 and 8	Israeli Arab	19	hom	g.44579C>G	c.2375C>G	p.P792R
9	Turkey	16	hom	g.38642–39025del388 bp	c.1936_2055del	p.E646_685del
10	Turkey	16	hom	g.38642–39025del388 bp	c.1936_2055del	p.E646_685del
11	Saudi Arabia	17	hom	g.40006_40084dup	c.2096_2174dup	p.E725fsX745
12	USA Native American	10	hom	g.31487_31488insC	c.1058_1059insC	p.I353fsX432
13	Canada	3	het	g.10097C>T	c.260C>T	p.P87L
		1	het	g.326_327insC	c.78_79insC	p.S27fsX54
14	Bahrain	18	hom	g42220C>T	c.2293C>T	p.Q765X
15	Belgium	14	hom	g.35409G>A	c.1724+1G>A	p.P535_L575del p.P535fsX625
16	Turkey	9	hom	g.24804C>A	c.888C>A	p.Y296X
17	Turkey	15	het	g.36360_36361insG	c.1827_1828_insG	p.W609fsX625
		18	het	g42220C>T	c.2293C>T	p.Q765X

[a]Kurdish ethnic group. NA, not available.

subunit in knockdown cells was verified by quantitative PCR analysis (Fig. 5A). Confocal microscopy of cells treated with *ATP6V0A2* siRNA and subsequently stained for Golgi markers Giantin and GM130 showed dispersed, vesicular morphology of the Golgi apparatus compared with continuous membrane structures in control cells (Fig. 5B). Electron microscopy (EM) showed tight Golgi stacks in control cells (Fig. 5C) and swelling of the cisternae in knockdown cells (Fig. 5D).

We next studied patient-derived skin fibroblasts under post-confluent conditions when the cells were actively secreting extracellular matrix. ARCL2 fibroblasts showed disruption and swelling of the Golgi apparatus by immunostaining (Fig. 6A, Patient 9) and EM (Fig. 6C and D, Patient 1), as we observed in the siRNA knockdown experiments. In addition, ARCL2 cells contained abundant autophagosomes (Fig. 6D and E) multivesicular bodies (Fig. 6E) and large lysosomes (Fig. 6C and E), which were not observed in control cells (Fig. 6B).

Preserved synthesis and function of key elastic fiber glycoproteins in ARCL2

Reduced or abnormal elastic fiber formation is a shared causative mechanism in all cutis laxa syndromes described to date (21). Elastic fiber biosynthesis requires a scaffold of fibrillin microfibrils and a family of extracellular cross-linking

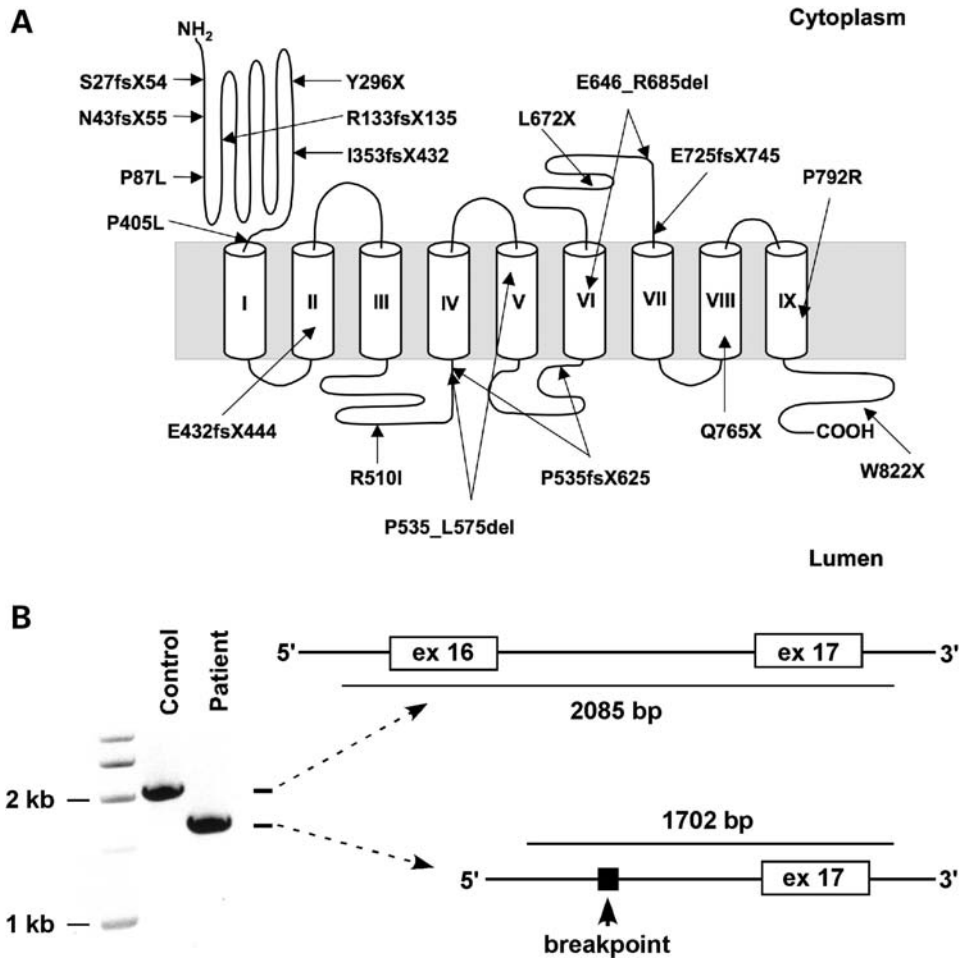

Figure 2. *ATP6V0A2* mutations in ARCL2 patients. (**A**) The location of each mutation is indicated on a membrane topology model of the ATPV0A2 protein. Predicted TM helices are shown by cylinders. (**B**) Mutation g.38643_39025del removes 388 bp of genomic DNA including exon 16 and surrounding intronic sequences.

enzymes, lysyl oxidases (LOXs) (22). Both fibrillins and LOXs are N-glycosylated. Thus, we tested if secretory abnormalities in ARCL2 interfered with the function of these key elastic fiber molecules. Immunostaining for fibrillin-1 showed normal density and morphology of microfibrils in all three ARCL2 fibroblast cultures tested. Representative fibrillin-1 staining is shown for a control and Patient 1 (Fig. 7A and B). LOX activity from concentrated conditioned media was slightly elevated in ARCL2, indicating that the synthesis and secretion of LOXs was also not impaired (Fig. 7C).

Abnormal elastin deposition in ATP6V0A2 mutant cells

Despite normal microfibrillar network and elevated LOX activity, elastin staining using an antibody against the alpha elastin fraction of insoluble elastin revealed a diminished elastic fiber network in all three ARCL2 fibroblast lines tested. Representative elastin staining is shown for Patient 1 (Fig. 7D and E). Quantitative assessment of insoluble elastin by metabolic labeling and biochemical isolation showed accelerating synthesis of insoluble elastin with culture time in control fibroblasts (Fig. 7F). Initially, ARCL2 fibroblasts were able to deposit low amounts of elastin, but later the mutant cells were not able to sustain high levels of elastin production. Similar results were obtained in three independent experiments. Normalization to either total ^{3}H-leucine incorporation into the cell layer (Fig. 7F), or to cell number, or to both (not shown) did not alter the results, showing that decreased elastin deposition was not caused by inefficient leucine uptake and utilization by ARCL2 cells or by reduced cell numbers.

In both control and patient cells, staining by antibodies against human recombinant tropoelastin (TE), the soluble precursor of elastin detected fibrillar material and globular pericellular aggregates (Fig. 7G and H), known to be intermediates of elastic fiber formation (23). In contrast, ARCL2 cells showed very little fibrillar elastin, and most immunoreactivity was found in globular TE deposits. Quantitative morphometry showed that the number of globular TE aggregates per cell was significantly increased in ARCL2 cells compared with controls (Fig. 7I).

Defective TE trafficking and secretion in ARCL2

In addition to the extracellular TE aggregates and fibrillar material observed (Fig. 7G and H), TE antibodies strongly stained intracellular vesicles including perinuclear structures

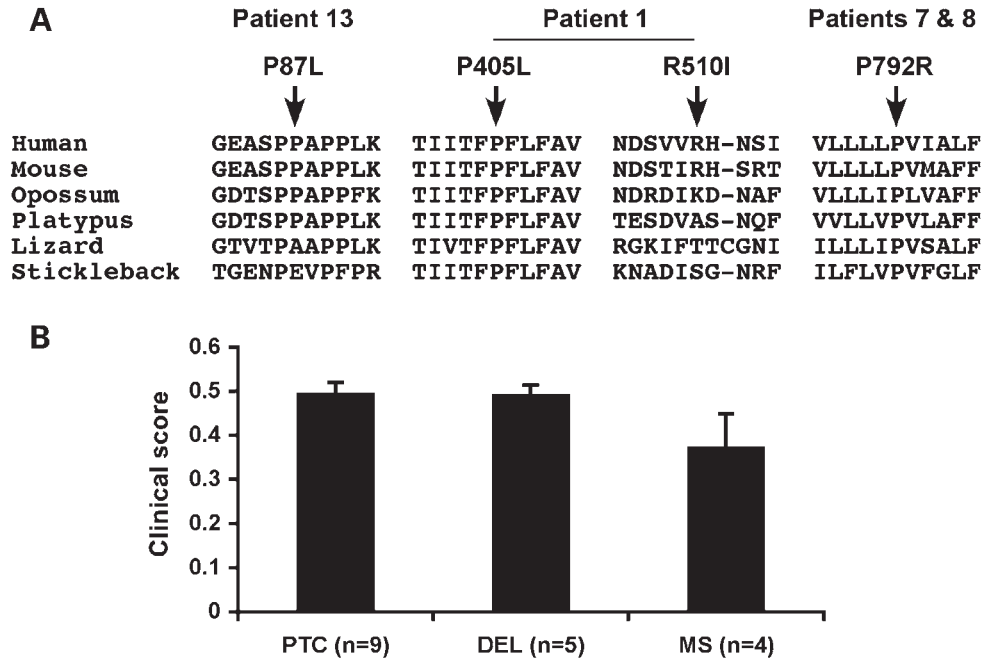

Figure 3. Missense mutations and genotype–phenotype correlations in ARCL2. (**A**) Phylogenetic conservation of residues affected by missense mutations. Multiple alignment of amino acid sequences for ATP6V0A2 from human (*Homo sapiens*), mouse (*Mus musculus*), opossum (*Monodelphis domestica*), platypus (*Ornithorhynchus anatinus*), lizard (*Anolis carolinensis*) and stickleback fish (*Gasterosteus aculeatus*) were generated using the University of California Santa Cruz Genome Browser (http://genome.ucsc.edu). (**B**) Mean clinical scores ($\pm$SEM) by mutation class. Data for patients with premature termination mutations on both alleles (PTC), patients with homozygous exon 16 deletion (DEL) or at least one missense mutation (MS) are shown. *t*-Tests showed no significant differences by mutation class ($P > 0.05$).

similar to the Golgi apparatus (data not shown). Dual immunostaining of control cells for the Golgi marker GM130 and TE showed colocalization in some (Fig. 8B), but not all, cells (Fig. 8A). This is consistent with the previously published observation that at a given time only a subset of cultured cells secrete TE (24). In contrast, most ARCL2 cells showed abundant TE staining in distended and fragmented Golgi sacs (Fig. 8C). In some ARCL2 cells, TE-containing Golgi vesicles merged to form a single large intracellular aggregate (Fig. 8D). The endoplasmic reticulum (ER) marker BiP/GRP78 did not show colocalization with TE in either control or ARCL2 cells (data not shown).

To provide further evidence for impaired TE secretion, we conducted pulse–chase immunoprecipitation experiments. After 4 h pulse labeling, control cells quickly accumulated labeled TE with a peak at 30 min chase (Fig. 8E), followed by a decline in intracellular TE, consistent with rapid secretion of TE (25). In contrast, ARCL2 cells continued to accumulate TE for up to 1 h chase. TE in the media of control cells rapidly increased, with a plateau after 15 min chase. Conversely, TE appeared in the media of ARCL2 cells more slowly (Fig. 8F).

Increased apoptosis in ARCL2

Some ARCL2 cells appeared to store large amounts of TE vesicles (Fig. 9A), consistent with our EM observations (Fig. 6E). TE storage was associated with an abnormal nuclear morphology characteristic of dying cells. TUNEL staining for apoptotic cells (Fig. 9B and C) showed $\sim$4% apoptosis rate in control cell lines, whereas 12% of ARCL2 cells were apoptotic (Fig. 9D), a highly significant difference. Notably, the cell density in ARCL2 cells was not reduced, suggesting that increased proliferation compensated for the loss of cells. This is consistent with a published report showing that fibroblasts producing reduced amounts of elastin have elevated proliferation rates (26).

DISCUSSION

Our studies provide molecular and clinical data on the largest group of ARCL2 patients described to date, providing the best estimate so far of the prevalence of each phenotypic component of this syndrome. In children diagnosed with *ATP6V0A2* mutations, we observed a relatively low frequency of growth delay, previously considered as one of the diagnostic hallmarks of ARCL2 (17). Even more interesting is the high prevalence of congenital eye anomalies in patients diagnosed with *ATPV0A2* mutations and ARCL2/WSS. The most common ocular abnormality is strabismus, a characteristic feature of congenital disorders of glycosylation. Therefore, we suggest prospectively screening children with ARCL2 for ophthalmologic anomalies.

Based on the current findings, the frequency of congenital brain anomalies in ARCL2 has been underestimated as well. We observed a spectrum of variable brain malformations, including white matter heterotopias, and other developmental defects from partial pachygyria to lissencephaly in several children. However, none of these brain malformations are specific for *ATP6V0A2* mutations because brain

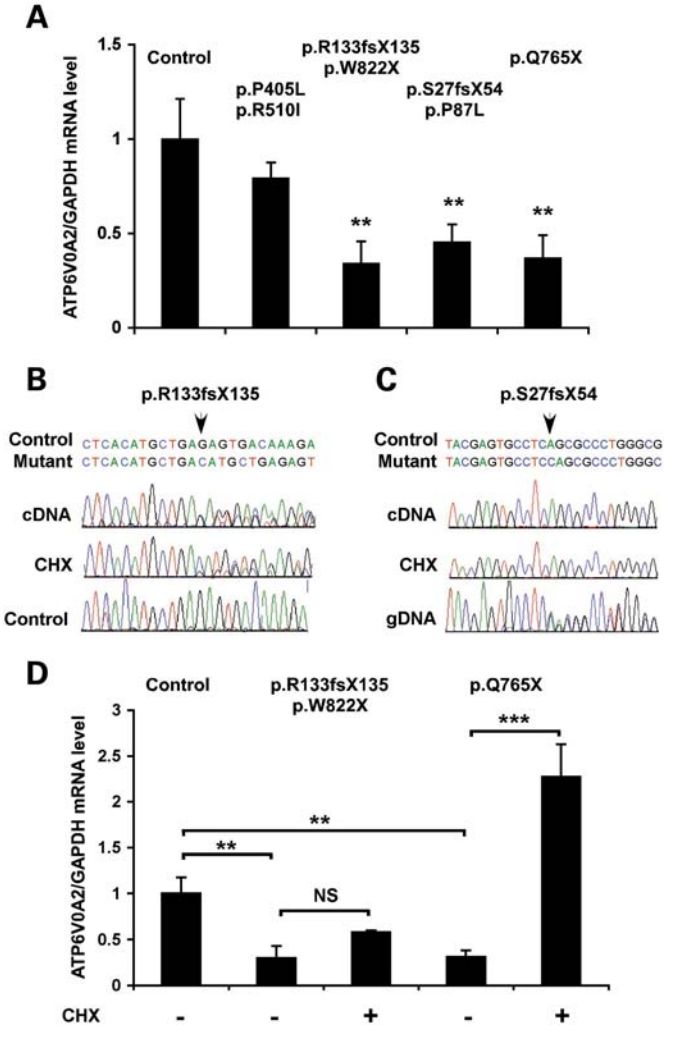

Figure 4. Reduced mRNA expression in *ATP6V0A2* mutant cells. (**A**) Relative expression of *ATP6V0A2* in skin fibroblasts of ARCL2 patients and normal individuals. GAPDH was used as an internal reference gene. Bars show means of three independent experiments, each with triplicate samples, error bars are standard error of mean (SEM). The frameshift and nonsense mutations showed significantly ($^{**}P = 0.01$, *t*-test) reduced *ATP6V0A2* expression compared with control individuals (average of five individuals). The mutations in each fibroblast sample are shown above the bars. Patient 1 who carried homozygous missense mutations showed a comparable *ATP6V0A2* expression to control subjects. (**B**) Skin fibroblasts from Patient 5, compound heterozygous for mutation p.R133fsX135 and p.W822X were cultured in the absence/presence of CHX and used as a source of RNA for reverse transcriptase-polymerase chain reaction (RT-PCR) experiments. RT–PCR products (cDNA) were subjected to direct DNA sequencing to monitor the expression of mutation p.R133fsX135, and sequence traces were aligned to a trace from a control sample. (**C**) Fibroblasts from Patient 14, compound heterozygous for mutations p.P87L and p.S27fsX54 did not express mutation p.S27fsX54 at the mRNA level, even in the presence of CHX. Sequence traces of the cDNA were aligned to the sequence of genomic DNA from the patient (gDNA) as a reference. The position of the mutation in each sequence alignment is shown by an arrow. (**D**) Quantitative RT–PCR analysis of *ATP6V0A2* mRNA expression in ARCL2 fibroblasts treated with CHX (+) or left untreated (−). GAPDH was used as an internal reference gene, and data were normalized to the mean of measurements from four control, untreated fibroblasts. Bars show means ± SEM of three independent experiments, each with triplicate samples, $^{**}P < 0.01$ and $^{***}P < 0.001$ (*t*-test).

malformations have also been reported in mutation-negative ARCL2 patients (18).

Liver function anomalies and coagulation defects have not been reported previously, except for sporadic cases with *ATPV0A2* mutations (12). Although the prevalence of these features is quite low, if present, they might predict a putative 'metabolic' subgroup of ARCL2. Additionally, one should emphasize the significance of screening with isoelectric focusing of both transferrin and apolipoprotein CIII in the diagnostic protocol of ARCL2. Even though the biochemical analysis for N-glycosylation has been shown to be normal in all patients tested during the first-half year of life (three patients so far), mucin type O-glycosylation was abnormal. After this initial period, abnormal N-glycosylation remains the best predictive marker for the underlying genetic disorder. Biochemical testing is especially important in cases with mild systemic involvement, such as Patient 13, where clinical diagnosis of ARCL2 is difficult.

A weak genotype–phenotype correlation was detected. The lowest clinical score was observed in Patient 13 who harbored a missense mutation (p.P87L) of a moderately conserved residue within the N-terminal, cytoplasmic portion of ATP6V0A2. The second lowest clinical score was found in Patient 1 who also carried a missense mutation. In contrast, the two patients who carried the missense mutation p.P792R that affects a highly conserved proline within a putative TM helix had a phenotype within the range found for most other mutations. In four patients of Middle Eastern origin, we detected a deletion of exon 16, which results in an in-frame deletion of a peptide encoding TM helix VI. The inevitable loss of function of the resulting protein is reflected by a relatively high clinical score (mean score = 0.49, range = 0.41–0.62). Children carrying truncating mutations (Patients 3, 5, 6, 11, 12, 14, 15, 16 and 17) had a similarly high score (mean score = 0.50, range = 0.41–0.65), correlating with a more severe clinical presentation. However, there was no statistically significant difference in clinical scores by mutation class.

We provide the first experimental evidence that *ATP6V0A2* mutations cause ARCL2 via a loss-of-function mechanism. This conclusion is supported by the high frequency of mutations that disrupt the reading frame, and significantly reduced *ATP6V0A2* mRNA levels in fibroblasts carrying PTC mutations. We also demonstrate that abnormal elastin biosynthesis is an important disease mechanism underlying ARCL2. We have shown that ARCL2 fibroblasts can elaborate normal microfibrillar scaffold and can secrete LOXs with normal activity. However, the assembly of elastic fibers was clearly defective in high-density cultures with low levels of insoluble elastin synthesis and the deposition of abnormal globular aggregates of TE.

Our electron microscopic and immunostaining studies suggest that the intracellular trafficking of TE-containing vesicles may be defective. This is supported by the swelling and fragmentation of the Golgi apparatus and the accumulation of abnormal, TE-positive Golgi vesicles in ARCL2 fibroblasts. We, furthermore, show that intracellular accumulation severely disrupts the secretion of TE. Interestingly, the ultrastructure of multivesicular bodies and lysosomes vesicles in

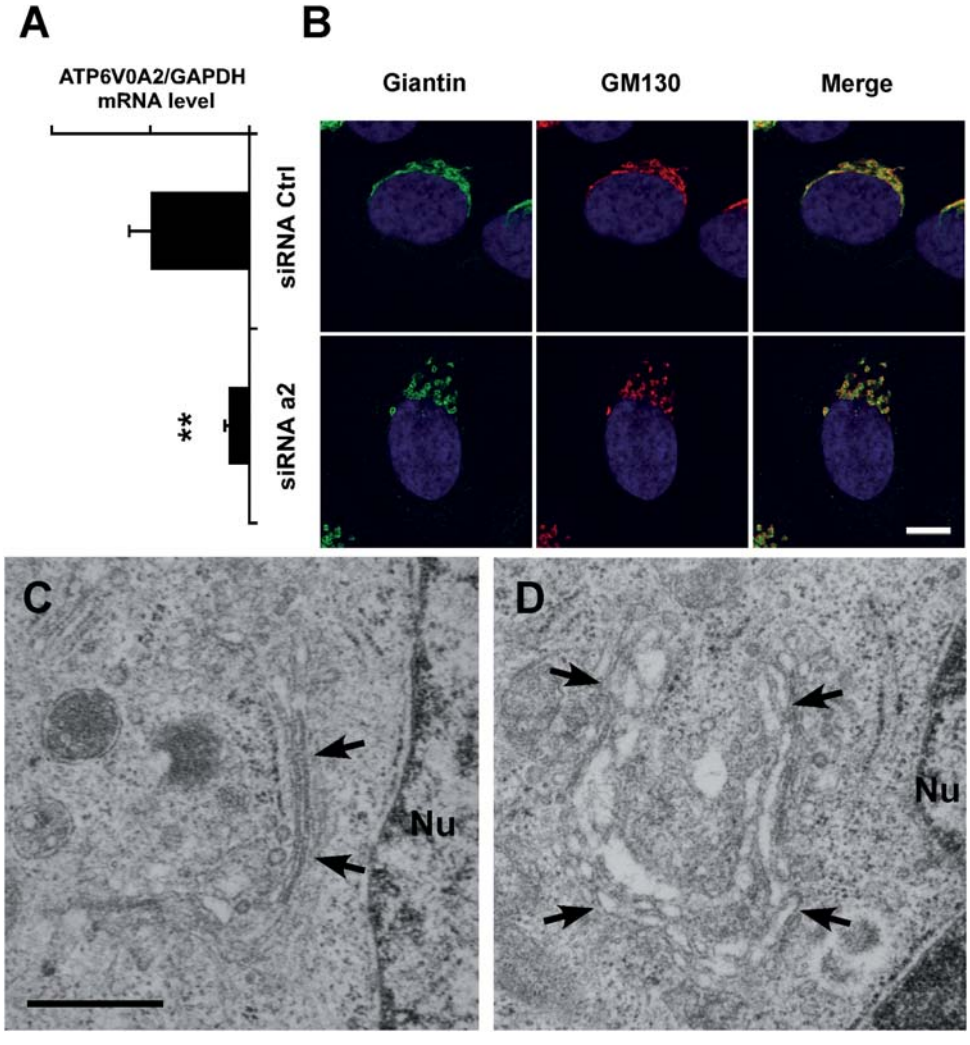

Figure 5. Golgi structure in HeLa cells after RNAi. (**A**) Quantitative RT–PCR analysis of *ATP6V0A2* mRNA expression in HeLa cells transfected with control (siRNA Ctrl) or *ATP6V0A2* siRNA (siRNA a2). Bars indicate means ± SEM, $^{**}P < 0.01$ (*t*-test). (**B**) Immunofluorescence staining of Golgi markers Giantin (green) and GM130 (red) in HeLa cells after siRNA treatment. Loss of *ATP6V0A2* (siRNA a2) induces disruption of the Golgi ribbon into mini-stacks. Magnification bar: 10 μm. EM of representative HeLa cells after siRNA-mediated knockdown of *ATP6V0A2* (**D**) shows abnormal morphology of the Golgi cisternae (arrows) compared with HeLa cells treated with a control siRNA oligonucleotide (**C**). Magnification bar: 0.5 μm.

ARCL2 cells is similar to those observed in the zebrafish mutant, 'catastrophe' caused by a mutation in the *atp6v0d1* gene encoding the d1 subunit of the vacuolar H^+-ATPase (27), highlighting the essential and general role of the vacuolar ATPase in vesicular trafficking, sorting and maturation (28–30).

Despite characteristic structural abnormalities of the secretory pathway, our results show that in ARCL2 cells, the production and function of several secreted glycoproteins including fibrillin-1 and LOXs are not affected. Fibronectin is known to be required for microfibril formation (31,32). Thus, the finding of abundant fibrillin-1 microfibrils in ARCL2 cell cultures suggests that, by extension, fibronectin function is also normal in ARCL2. Preserved LOX activity in ARCL2 cells is particularly relevant in comparison to the 'catastrophe' mutant, which exhibits pigmentation and notochord defects under limited Cu^{2+} availability, consistent with impaired cuproenzyme activity. Notochord defects are characteristic of functional deficiency of LOXs (33). Taken together, these findings demonstrate that mutations in different subunits of the vacuolar H^+-ATPase can lead to defects in the trafficking of specific secretory proteins. In 'catastrophe', an *atp6v0d1* mutation results in reduced LOX activity, whereas, in ARCL2, *ATP6V0A2* mutations result in preserved LOX activity but impaired TE trafficking.

Past studies of cellular trafficking of TE suggest that this protein utilizes a constitutive secretion pathway with rapid release of newly synthesized TE into the extracellular space (24). This process was shown to be dependent on an acidic vesicular compartment and could be inhibited by the vacuolar H^+-ATPase inhibitor bafilomycin, or by treating the cells with ammonium chloride, a chemical that neutralizes acidic vesicles (24). The specific sensitivity of TE secretion to reduced vesicular acidity may be related to the aggregation properties of this protein. TE has a unique ability to undergo a spontaneous phase transition, called coacervation, which yields a high concentration protein aggre-

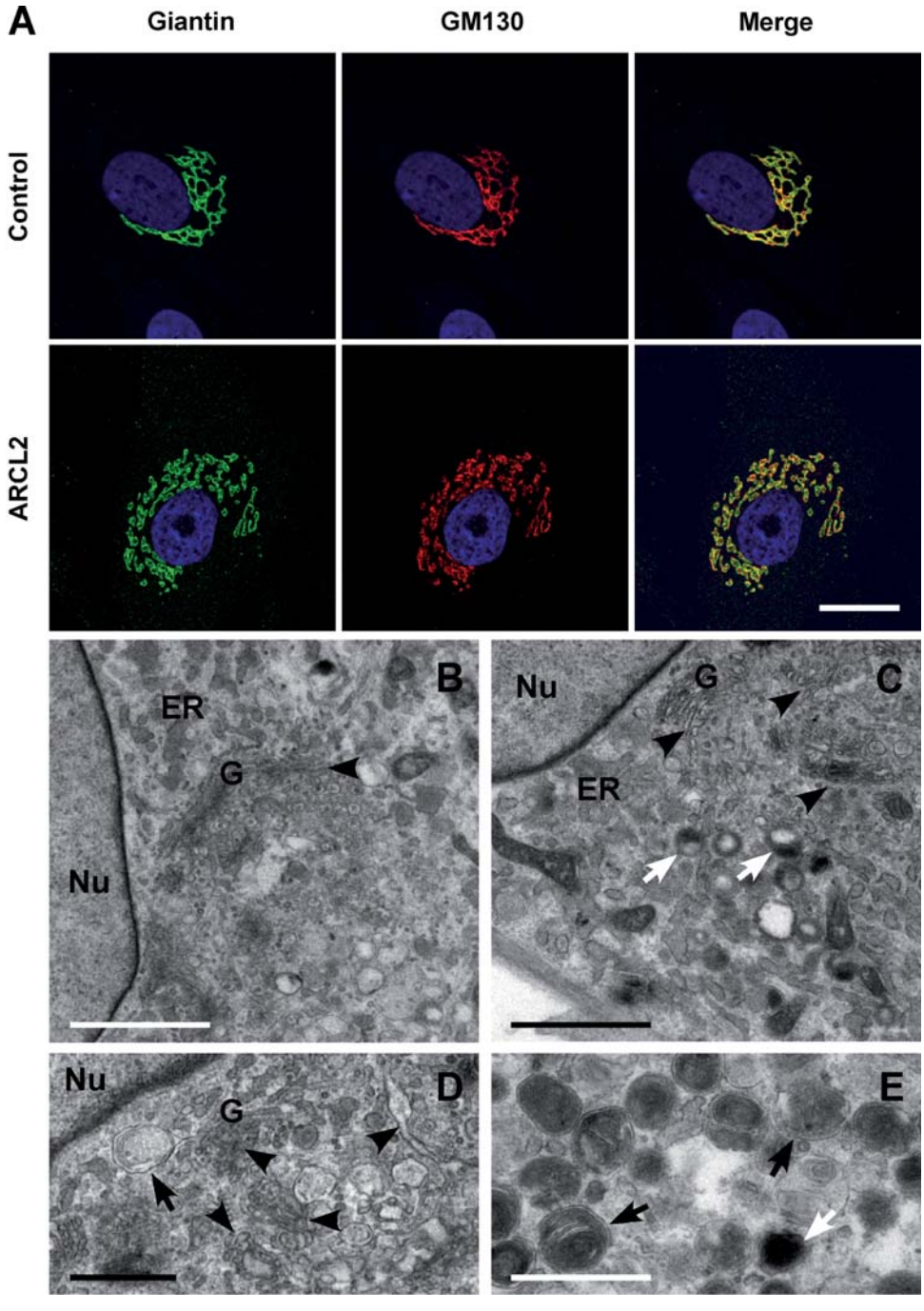

Figure 6. Abnormal secretory apparatus in ARCL2 fibroblasts. (**A**) Immunofluorescence staining of Golgi markers Giantin (green) and GM130 (red) in extracellular matrix-secreting fibroblasts from ARCL2 Patient 9 shows disruption of the Golgi ribbon into mini-stacks compared with well-organized Golgi apparatus in control cells. Transmission electron microscopy of representative control (**B**) and ARCL2 (**C**–**E,** Patient 1) fibroblasts shows normal morphology of the nucleus (Nu) and the endoplasmic reticulum (ER). In contrast, the Golgi apparatus (G) in ARCL2 cells shows abnormal swelling and fragmentation (C and D, arrowheads). In addition, ARCL2 fibroblasts contained many lysosomes (C and E, white arrows) and autophagosomes and multivesicular bodies (D and E, black arrows). Magnification bars A: 10 μm; B and C: 2 μm; D and E: 1 μm.

gate. Increasing TE concentration, ionic strength, temperature and pH facilitate coacervation (34). This process is thought to be essential for elastin assembly in the extracellular space. At neutral pH, coacervation occurs at body temperature (37°C), whereas at the acidic pH present in normal secretory vesicles (pH 5.7) the coacervation temperature is 40°C (34). This property ensures prompt coacervation upon release to the extracellular matrix but keeps TE in solution in secretory vesicles at body temperature. Loss of ATP6V0A2 is likely to lead to elevated vesicular pH and premature aggregation of TE, which may interfere with the trafficking of secretory vesicles within and distal to the

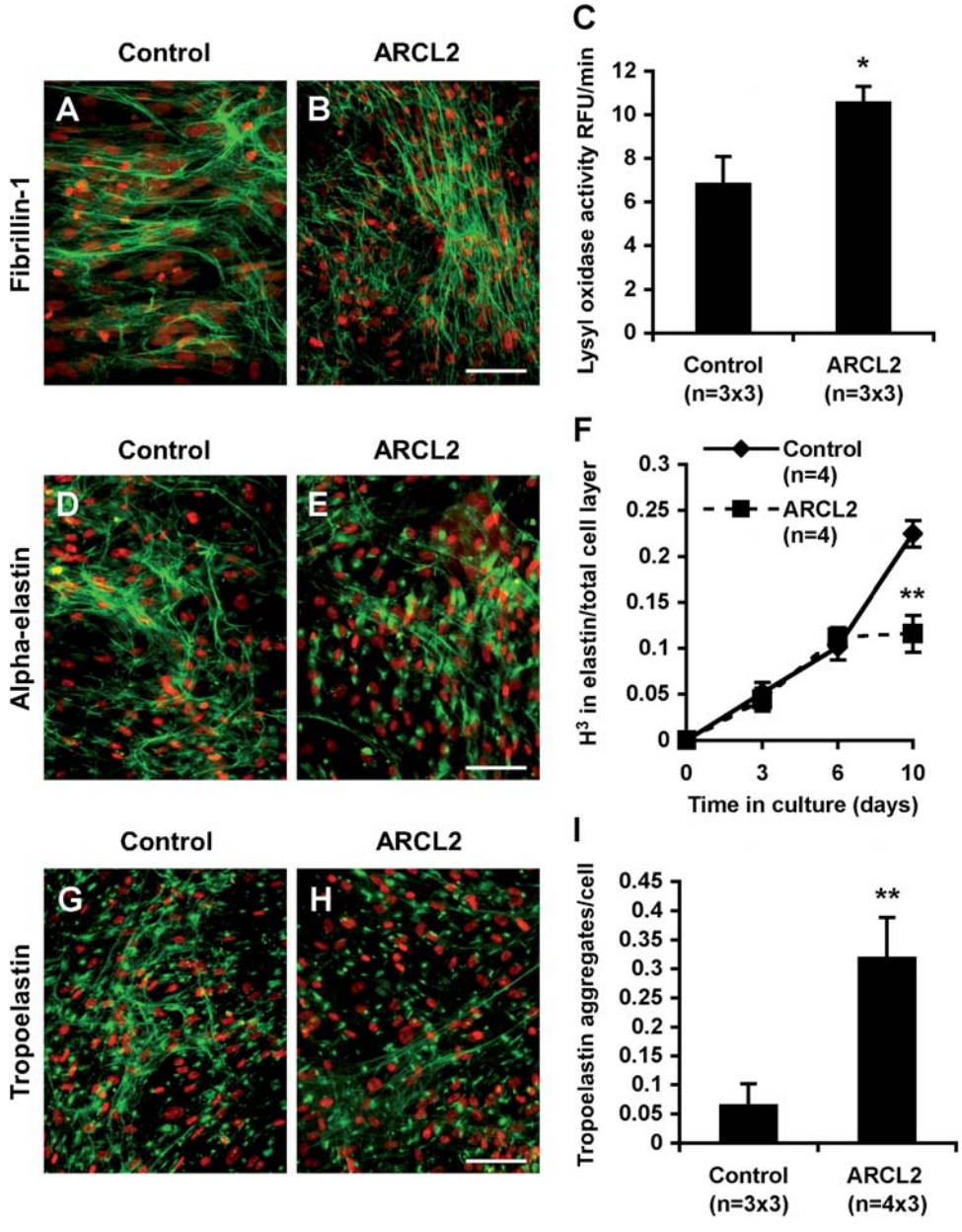

Figure 7. Specific disruption of elastin biosynthesis in ARCL2 cells. Fibroblast cultures from a control individual (**A, D** and **G**) and from Patient 1 (**B, E** and **H**) were immunostained for fibrillin-1 (A and B) α-elastin (D and E) and TE (G and H). Nuclei were counterstained with propidium iodide (red). Magnification bars: 50 μm. (**C**) LOX activity in concentrated conditioned media was measured using the amplex red fluorescence assay as activity inhibitable by BAPN. Means show triplicate samples from three control and three patient fibroblasts, respectively, ± SEM. $^{*}P < 0.05$ (*t*-test). (**F**) Skin fibroblasts of the patients and control subjects were labeled with ^{3}H-leucine, and elastin was isolated by boiling in 0.1 N NaOH. The insoluble elastin obtained this way was hydrolyzed and ^{3}H-leucine incorporation was quantified by scintillation counting. The results were normalized to the total radioactivity incorporated into insoluble proteins in the cell layer. Data points show means of four fibroblast lines for each group ± SEM. $^{**}P < 0.01$ (*t*-test). (**I**) Quantitative analysis of globular elastin aggregates was based on staining of three control cell lines and four ARCL cell lines. Three low power fields were used for counting in each line, and results were averaged by group. Bars indicate means ± SEM, $^{**}P < 0.01$ (*t*-test).

Golgi, resulting in the accumulation and abnormal morphology of vesicles we observed by EM and immunostaining. Alternatively, the formation of a secretory carrier could be impaired due to defective recruitment of ADP-ribosylation factors that are known to bind Golgi membranes in a pH-dependent manner (35). The inability to turn over TE-containing secretory vesicles may in time lead to cell death and release of vesicles into the extracellular space. This notion is supported by the observed accumulation of vesicular material containing TE in ARCL2 cells, the increased number of globular TE aggregates and the increased rates of apoptosis in ARCL2 cells.

Although it is not necessary to invoke abnormal glycosylation to explain the observed TE aggregation in the Golgi, recent studies show that removal of sialic acid residues from glycoconjugates in the extracellular matrix accelerates

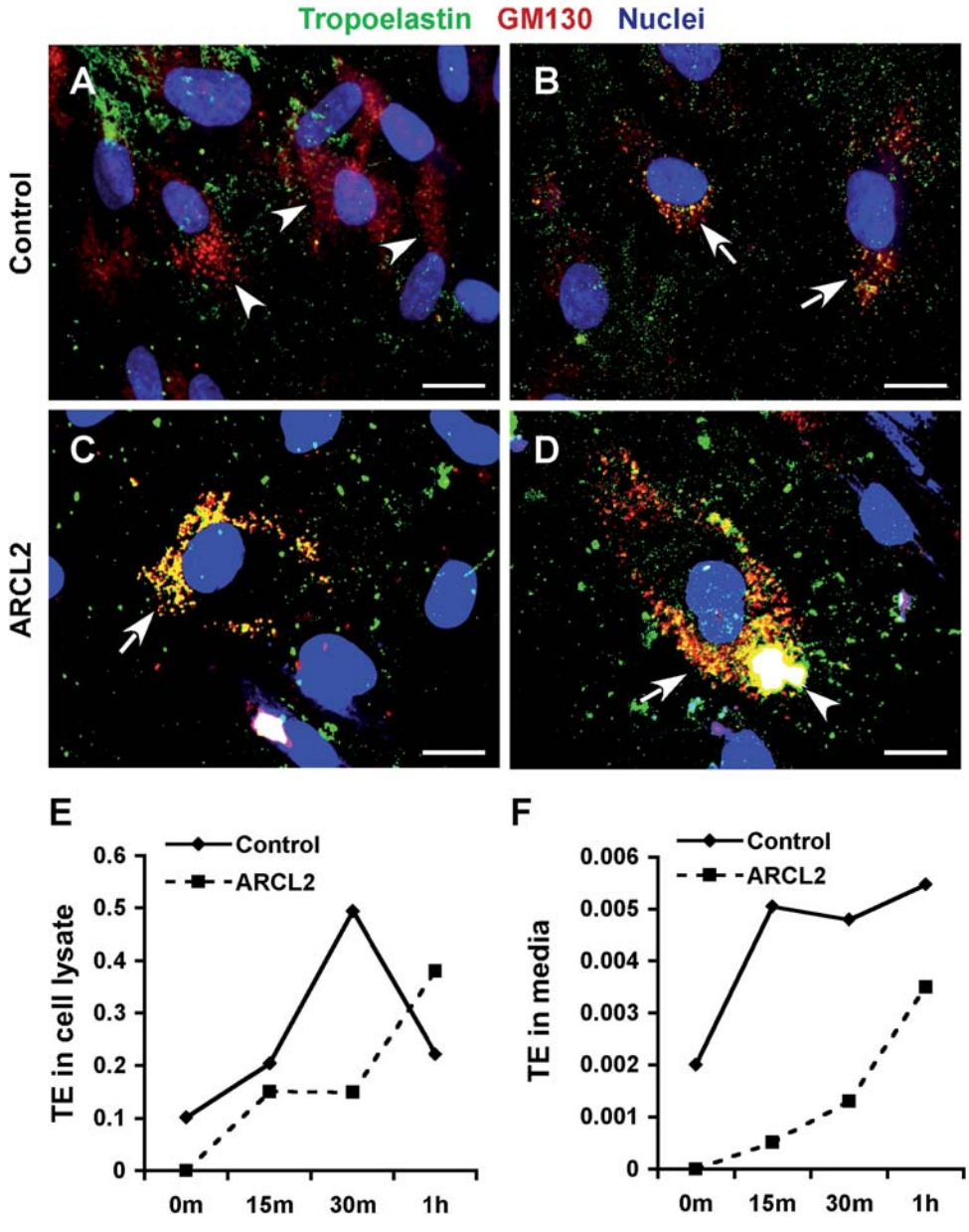

Figure 8. Impaired secretion and accumulation of TE in Golgi vesicles. Dual immunostaining for TE (green) and Golgi marker GM130 (red) in control cells commonly showed well-developed Golgi stacks (**A,** arrowheads) that were negative for TE. Golgi structures in a few control cells were positive for TE (**B,** arrows) showing fine vesicular and compact perinuclear morphology. In contrast, in ARCL2 cells (Patient 2), distended Golgi vesicles were highly positive for TE (**C** and **D,** arrows). In some cells, TE-positive Golgi sacs merged to form large intracellular aggregates (**D,** arrowhead). Magnification bars: 10 μm. Pulse–chase immunoprecipitation of TE from fibroblast lysates (**E**) showed rapid synthesis and secretion of TE in control cells, but continuous intracellular accumulation of TE in ARCL2 cells (Patient 1). TE, the media (**F**) rapidly reached maximal levels in control cells, accumulated slowly in ARCL2 cells (m = minutes and h = hours).

elastin deposition, and animals or cells deficient for silaidase (neuraminidase-1) show abnormal elastin deposition (36,37). Thus, it is possible that reduced sialylation of an as yet uncharacterized glycoprotein chaperone may contribute to the premature aggregation of TE in the Golgi by replicating a glycan milieu similar to the extracellular space.

Abnormal elastin biosynthesis and increased apoptosis of fibroblasts readily explains cutis laxa and connective tissue phenotypes associated with ARCL2 but is an unlikely cause of the neurodevelopmental and growth defects associated with this disease because elastin is not known to be required for brain or bone growth. However, our results suggest that impaired secretion of specific brain or bone proteins with similar biochemical properties to TE may be considered as a potential mechanism underlying the neural and skeletal defects in ARCL2.

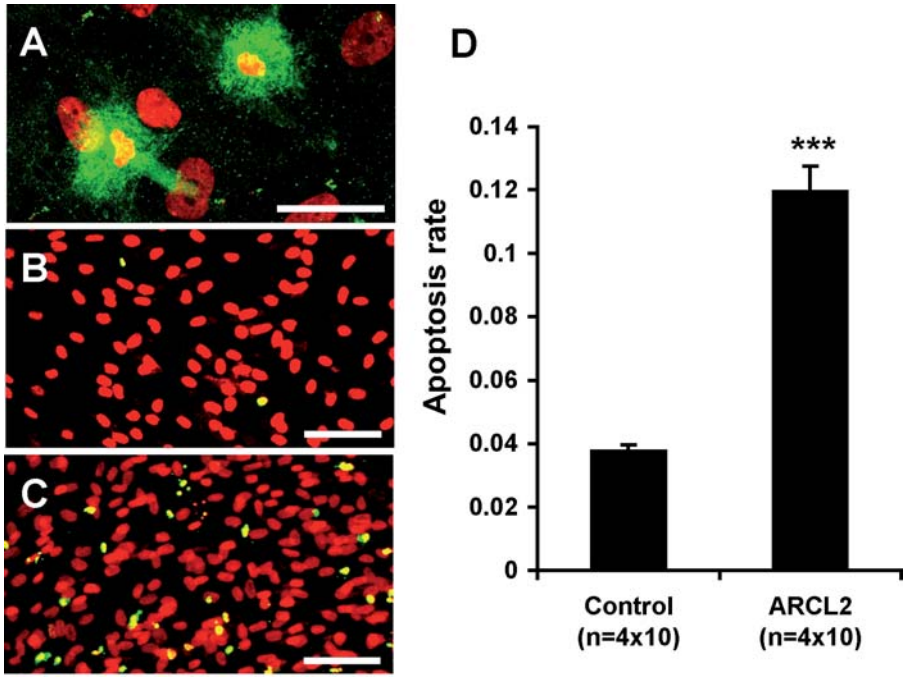

Figure 9. Increased apoptosis in ARCL2. Immunostaining of ARCL2 cells (Patient 1) showed intracellular accumulation of vesicular material highly positive for TE and abnormal nuclear morphology characteristic of cell death (**A**). Representative micrographs of control (**B**) and ARCL2 (**C**) fibroblasts subjected to TUNEL staining (green) to visualize apoptotic nuclei, nuclei were counterstained with propidium iodide (red) yielding a yellow color for apoptotic nuclei and red for normal nuclei in merged images. Magnification bars: A, 20 μm; B and C, 50 μm. (**D**) Quantitative analysis of apoptosis rate (apoptotic nuclei/all nuclei) was applied to four control and four ARCL2 cell lines with 10 microscopic fields analyzed for each line. Bars indicate means ± SEM, $^{***}P < 10^{-12}$ (*t*-test).

MATERIALS AND METHODS

Subjects

The patient, parents and normal control individuals participated in this study following informed consent. This study has been approved by the Human Studies Committee of Washington University School of Medicine. Tissue samples were collected as skin biopsies. Normal control tissue samples were provided by the Cooperative Human Tissue Network, which is funded by the National Cancer Institute. Other investigators may have received specimens from the same subjects. Control DNA was obtained from normal volunteers of diverse ethnic backgrounds. DNA was isolated from peripheral blood or dermal fibroblasts by isolating nuclei, followed by proteinase K digestion and phenol extraction (38).

Clinical evaluation

The following clinical features have been evaluated and scored according to the involvement of organs and organ systems, functional and laboratory anomalies: skin, congenital cutis laxa/wrinkled skin; skeletal, large fontanelles or delayed closure; brain/neurocranium, microcephaly, partial pachygyria; joints, congenital hip luxation, joint laxity; connective tissue, hernias; heart, congenital cardiac anomalies; urinary system, congenital urogenital anomalies; CNS function, seizures, developmental delay; growth, small for gestational age or delayed growth; liver, liver function anomalies; coagulation, coagulation anomalies.

Glycosylation studies

In available serum samples, protein N-glycosylation and mucin type O-glycosylation was studied by isoelectric focusing of transferrin and apolipoprotein CIII, respectively, as described previously (39).

Mutational analysis

Intron-derived primers for PCR amplification of all 20 *ATP6V0A2* exons (Table 4) were synthesized using sequence information obtained from the reference sequence (GenBank accession number NT_009755). Intron/exon boundaries were deduced from information available in the Ensembl database and by comparison with the *ATP6V0A2* cDNA (GenBank accession number NM_012463). Primers were designed using the Vector NTI advance program version 9.1, on the basis of the annotated genomic sequence across each exon, including regions of at least 80–100 bp of flanking intervening sequence. Larger exons were subdivided to allow for optimal product lengths, whereas small exons and intronic regions were grouped into single optimal product. PCR amplifications were performed in a 25 μl volume with 100 ng of genomic DNA, 25 μM of each primer, 200 μM dNTPs, 10 mM Tris, pH 8.0, 50 mM KCl, 1.5 mM $MgCl_2$ and 0.125 U of AmpliTaq GOLD DNA polymerase (Applied Biosystems, Foster City, CA, USA). Conditions for PCR were 10 min of initial activation step at 95°C, followed by 35 cycles of denaturation at 95°C for 30 s and annealing at 62°C for 30 s, and an extension at 72°C for 30 s and a final 7 min extension at 72°C. An

Table 4. Oligonucleotides for the amplification of *ATP6V0A2* exons

Exon	Forward primer	Reverse primer	Size
1	TGCAGTCTGGAGCCCCATAGTG	TGTCATCTTCCCCGTCTGGACAA	398
2	AGGGTTGGGGTTTCACCGTGTT	GGGTAACAACAAAATAACCAGGCCAT	526
3	ACCAGTAAGTCAGTTGGGACAAGCA	TGCCTAGAGAGATCACCATCTTCCA	377
4	ACCCACTGTTTTTGGTATACTGCAT	AATACACAGCCTATGGGAATGAGAT	310
5	CCTCAGAAGTCTTTGCACCCAGAT	TCCATTCATCCCTTCTATGGAGCT	302
6	GGCTCTCAGGATGTCTTCACCACT	CGTGGTTGAAGAGATAAGGCATCA	375
7	CGCTCCGTGGATTGGTTTGG	GCAGCCACTCTATTTCTGACTCCAGA	368
8	TCTGTATGCACAGCCCGACCAA	GGAGGAGGGAGGGAAGCAACA	405
9	CCTCTGTCAATGGGGAGAAA	ACACAGCAAAACCCCATCTC	497
10	TGAGCCGAGATCACACCATT	TGGTCAGCCTCTCTTTCCAA	436
11	TGGAAAGAGAGGCTGACCATTACT	ACAGCCGCAGCCTACAGCAA	425
12/13	TGAGAAGTGAGTGGTGAGGGTCGT	GCGTGAACCCTGCTCAACAGTCTA	569
14	CCATCTGGCACCCTTTGACGT	TGCCCCTTACCCAATAAATACAGTCA	448
15	TTGGCCGACCTCACGTCTCT	TCACCCCAACACTTCTACTGCTCA	478
16	GAATGTTCCTCGCGTGGAGACA	AAGAGACAGGGACCCTCCAGGA	335
17	AGCCACTGTGCCTAGCCTAA	CAGAAATCCCACTGGCGAAGTGA	491
18	TGCGTCTGGGGTTTCTGTTCCT	ATCCCACAGTGCCCCCTGAGT	346
19	TGGGATAATAGTTCAGGGCCGTCA	TATTTGGTTGGGCGGGGCAGT	356
20	TGGAATGAAGCAATTTCAGCACA	TGGCTATGTCATAAGGCAGTAATGA	338
RT–PCR			
1–6	ATGTGCCTGGCGCAGCTCTT	TGCATAGGACACGATGGTGTACCCT	588
1/2–5	TCCAGTTCCGAGACCTCAACCA	TTGCTCCCAGCCTCTGCATACA	411
16–20	TGGCTTCACAATGGGCGTAGT	TCATGCCACACTGTCGTCGTT	555
17–20	GTTTCATTGCTGGGAAGCCAAGA	TTGGTGCCTGCACCAACGTAGA	413

Size = size of PCR products in base pairs. Annealing temperature was 62°C for all amplifications except exon 1 at 65°C, exon 10 at 64°C and exon 17 at 69°C. RT–PCR primers were annealed at 60°C.

annealing temperature of 65°C was used for PCR amplification of exon 1, 64°C for exon 10 and 69°C for exon 17.

Purified PCR-amplification products were sequenced using BigDye-terminator chemistry and were electrophoresed on ABI 3730XL (Applied Biosystems) using the manufacturer's standard protocol and reagents. Sequence analysis of both the sense and antisense strands of the PCR-amplified fragments was performed with the aid of Sequencher 4.5 software (GeneCodes, Ann Arbor, MI, USA). Sequence electropherograms were compared with the reference gene sequences. DNA sequencing of two independent amplification products confirmed mutations. To rule out polymorphisms, observed variants were compared with single nucleotide polymorphism databases.

RNA studies

Fibroblasts were cultured to confluency at passages 2–8 in Dulbecco's modified Eagle's medium (DMEM) supplemented with 10% fetal bovine serum (FBS), 25 mM HEPES, L-glutamine and antibiotics. Parallel cultures were set up with the addition of 100 μg/ml CHX for 4 h prior to RNA extraction to study nonsense-mediated decay. Confluent cultures were used to extract RNA using TRI-reagent (Molecular Research Center, Cincinnati, OH, USA), following the manufacturer's protocol. First strand cDNA was synthesized from total RNA samples (1 μg each) using SuperScript III reverse transcriptase (Invitrogen, Grand Island, NY, USA). The amplification conditions included an initial denaturation at 65°C for 5 min, then a primer-annealing phase at 25°C for 10 min, an extension phase at 50°C for 50 min and an enzyme denaturation step at 85°C for 5 min. We performed reverse transcriptase–polymerase chain reaction (RT–PCR), using the cDNA templates to amplify desired regions (Table 4) of *ATP6V0A2*, for the determination of splicing changes from the intronic and frameshift mutations. After visualization on a 1.2% agarose gel, products were purified using the QIAquick gel extraction kit (Qiagen, Valencia, CA, USA), reamplified and then were subjected to direct sequencing. PCR primers were designed at least one exon away from the mutation under study to prevent amplification of potentially contaminating genomic DNA.

Quantitative PCR

We measured relative RNA expression levels, using quantitative PCR with cDNA templates synthesized from 1 μg RNA. We performed these reactions using iQ SYBR green supermix and an iCycler iQ PCR System (Bio-Rad, Hercules, CA, USA). To measure *ATP6V0A2* expression, we used two assays, one spanning exon 1 (5′-TCCAGTTCCGAGACCTC AACCA-3′) to exon 3 (5′-CTTCAGGAAGGGGAATATCA GCTCT-3′), the other spanning exon 6 (5′-TGCAG AACTGGATGAATCCCTTGA-3′) to exon 8 (5′-ACGTGG CAGTGGTAGCAATCACA-3′). GAPDH was used as a reference transcript. Three independent experiments were performed, each in triplicates. 'No RT' samples were used as a PCR control measure for gDNA contamination. We performed $\Delta\Delta C_t$ analysis to assess the relative RNA expression levels, by first calculating the difference between the threshold cycle number (C_t) values of the target gene (*ATP6V0A2*) and the C_t value of the corresponding reference *GAPDH* gene. These calculations were then expressed in relation to the calibrator, which was arbitrarily set at an expression level of 1.00.

HeLa cell culture and siRNA treatment

HeLa cells were cultured at 37°C and 5% CO_2 in growth medium (DMEM containing 10% FCS and 2 mM glutamine). Cells were seeded into 6-well plates on glass coverslips 12–24 h before siRNA transfection. For transfection, 20 nmol of control (siRNA ID: AM4635, Applied Biosystems) and *ATP6V0A2* (siRNA ID: 20328, Applied Biosystems) annealed siRNA was transfected by INTERFERin (Polyplus-transfection, Illkirch, France) according to manufacturer specifications. After 12 h, a second transfection was performed and after 24 h, the cells were used for assays.

Immunocytochemistry

Cells were plated on coverslips in 6-well plates and grown 5–10 days past confluency. Post-confluent cultures were then washed with PBS once and were fixed in 4% paraformaldehyde in PBS at 4°C for 30 min. After several washes in PBS, cell cultures were incubated in 3% BSA in either Tris-buffered saline (TBS, 20 mM Tris–HCl, pH 7.4 and 0.15 M NaCl) for non-permeabilized cells or TBS/0.1% Triton X-100 for permeabilized cells for 1 h. For visualization of Golgi markers, permeabilization was performed in 3% BSA in 1× PBS with 0.1% saponin for 10 min. Cells were incubated with primary antibodies against human recombinant TE [PR398, Elastin Products Company (EPC), Owensville, MO, USA], human aortic alpha elastin (PR533, EPC), a recombinant C-terminal peptide of fibrilin-1 (a kind gift of Dr Robert P. Mecham), GM130 or BiP/GRP78 (BD Transduction Laboratories™), or Giantin (Covance, Emeryville, CA, USA) overnight. After several washes, cell cultures were incubated with secondary antibodies: anti-rabbit Alexa Fluor 488 and anti-mouse Alexa Fluor 555 or Alexa Fluor 594 (Invitrogen). Nuclei were stained with propidium iodide (Sigma, St Louis, MO, USA) or 4′,6-diamidino-2-phenylindole (DAPI) (Invitrogen). Cells were washed and then mounted with Gel/Mount (Biomeda, Foster City, CA, USA) or Fluoromount (Southern Biotech, Birmingham, AL, USA), and visualized with an Axioskop BX60 fluorescence microscope (Zeiss, Thornwood, New York, NY, USA) or an LSM 510 meta confocal microscope (Carl Zeiss, Göttingen, Germany) with a ×63 Plan Apochromat oil immersion objective.

Electron microscopy

For EM, cultured skin fibroblasts or HeLa cells were fixed in glutaraldehyde, stained sequentially with OsO_4 and uranyl acetate, then dehydrated and embedded in Epon (40). Thin sections (60 nm) were cut, placed on formvar-coated grids and counterstained with 7% methanolic uranyl acetate and lead citrate. Sections were viewed using a Tecnai 12 transmission electron microscope at 120 kV and images were digitally captured.

LOX assay

Measurement of activity was performed using the Amplex red fluorescence assay (41). This method utilizes the oxidation of Amplex red by hydrogen peroxide catalyzed by horseradish peroxidase where resorufin, a fluorescent product, is generated. As LOX produces H_2O_2, the fluorescence intensity is proportional to its activity. Fibroblasts were cultured to confluency and then incubated in phenol-red-free medium (Invitrogen Corporation, Carlsbad, CA, USA) for 48 h. The medium was collected and concentrated using centrifugal filters (Amicon Ultra-15, 10 kDa, Millipore, St Charles, MO, USA) at 2500 rpm for 2 h at 4°C. To verify the linearity of the assay, a standard hydrogen peroxide dilution series was prepared providing 100 µl of the final concentrations of H_2O_2: 0, 0.4, 0.8, 1.2, 1.6 and 2.0 µM. Concentrated protein samples were used as triplicates in a final volume of 120 µl. To completely inhibit LOX activity, parallel samples were prepared with 500 µM β-aminopropionitrile (BAPN) added. Finally, 30 µl of LOX 4× reaction buffer providing a final concentration of 1.2 M urea, 50 mM sodium borate (pH 8.2), 40 mM cadaverine, 4 U/ml horseradish peroxidase and 40 µM Amplex Red were added to each standard and sample well. The reactions were incubated at 37°C for 30 min, and the fluorescence was measured using a fluorescent plate reader (Tecan) at 37°C with excitation and emission wavelengths at 560 and 590 nm, respectively, 12 times, every 15 min. Fluorescence results of BAPN-treated samples were subtracted from untreated samples, and the reaction speed defined as relative fluorescence unit change per minute (RFU/min) was determined for each replicate by linear regression. Mean reaction speed values were determined for all replicates within each group (patient and controls), and Student's *t*-test was used for statistical analysis.

Insoluble elastin assay

Skin fibroblasts from four patients and four age- and sex-matched control subjects were plated on 60 mm cell culture dishes (100 000 cells/dish) and were grown to confluency. Then, 20 µCi of ^{3}H-leucine (Sigma) was added to each dish with fresh media. Cultures were incubated over a time course of 10 days and replenished with fresh media and radioactive leucine at days 3 and 6. At each time point, days 3, 6 and 10, the cultures were terminated and assayed for insoluble elastin as described previously (26,42). Briefly, after the removal of culture media, cell layers containing insoluble elastin deposited in the extracellular matrix were washed in 0.1 M acetic acid and then scraped in 0.1 N NaOH and centrifuged. The pellets were boiled for 45 min in 0.5 ml of 0.1 N NaOH to dissolve all extracellular matrix components except elastin. After centrifugation, the supernatants were saved to measure the radioactivity incorporated into total non-elastin insoluble proteins. The pellets containing the insoluble elastin were then hydrolyzed by boiling in 200 µl of 5.7 N HCl for 1 h, and the aliquots mixed with scintillation fluid and counted. A parallel set of cultures were grown under the same culture conditions except the presence of ^{3}H-Leucine and used to count the cell numbers at each time point and for DNA determination by the DNeasy Tissue system (Qiagen). Final results reflecting the amounts of metabolically labeled insoluble elastin were expressed as counts per minute per total number of cells or counts per minute per total labeled insoluble proteins.

Pulse–chase immunoprecipitation of TE

Fibroblasts from patients and normal samples were grown in 60 mm culture dishes. Three days after confluency, cells were incubated in leucine-free medium containing 5% dialyzed FBS for 1 h prior to metabolic labeling with 20 μCi/ml of ^{3}H-leucine. After 4 h of metabolic labeling (pulse), the cell layer was washed twice with warm PBS, and fresh DMEM media without FBS was added to each dish and chased for 0, 15, 30 min and 1 h time points. The chased medium was collected immediately for the first time point (0 min), and cell layer was washed three times with cold PBS and incubated with 1 ml of cold lysis buffer [25 mM Tris–HCl (pH 7.5), 5 mM EDTA (pH 7.5), 250 mM NaCl, 0.1% Triton X-100] with protease inhibitors (Sigma) for 30 min at 4°C on a platform shaker. Cells were pelleted by centrifugation, and the cell lysate was transferred in to clean tubes. The medium and lysates were processed for the subsequent time points and was immunoprecipitated with PR398 (Elastin Product Company, MO, USA) primary antibody over night at 4°C with gentle agitation. The following day, 40 μl of Pansorbin (EMD Chemicals, Gibbstown, NJ, USA) suspension was added to each tube and further incubated for 1 h at 4°C with gentle agitation. The immune complexes were pelleted and the pellets were washed twice with lysis buffer and once with non-detergent buffer [10 mM Tris–HCl (pH 7.5), 5 mM EDTA (pH 7.5)]. After, the final wash, the pellets were suspended in 1 ml scintillation liquid and measured for radioactivity using a Beckman LS 6000 K scintillation counter. Raw counts for immunoprecipitates were normalized to the activity of aliquots of the media and cell lysates prior to immunoprecipitation.

TUNEL assay

Apoptotic cells were stained using ApopTag fluorescein direct *in situ* apoptosis detection kit (Chemicon, Temecula, CA, USA) according to the manufacturer's instructions. Briefly, fibroblasts were grown on coverslips in 6-well plates. Confluent cultures were fixed in 1% paraformaldehyde in PBS for 10 min at ambient temperature (AT). Following two washes in PBS for 5 min, cell cultures were post-fixed and permeabilized in pre-cooled ethanol:acetic acid (2:1) for 5 min at −20°C and then washed in PBS three times. For positive controls, cell cultures were incubated in DNase buffer (30 mM Tris–HCl, pH 7.2, 4 mM $MgCl_2$, 0.1 mM DTT) for 5 min at AT. Then, 150 μl DNaseI working solution (1000 U/ml) was applied to positive control samples for 10 min at AT. Cell cultures were rinsed with five changes of water for 3 min each change. Samples were incubated in equilibration buffer for 10 s, and then immediately 110 μl of working strength terminal deoxynucleotidyl transferase enzyme was applied and incubated at 37°C for 1 h in a dark humidified chamber. The reaction was stopped by incubation in stop/wash buffer for 10 min at AT. Coverslips were mounted using Antifade (Chemicon) containing 0.5 μg/ml propidium iodide and visualized with an Axioskop BX60 microscope (Zeiss). To calculate the rate of apoptosis, 20 fields, arranged in a matrix of 4 × 5, of 10× magnification were taken from each slide. Numbers of total cells (propidium iodide positive) and apoptotic cells (fluorescein positive) were counted. Student's *t*-test was used for statistical analysis.

ACKNOWLEDGEMENTS

We thank the patients and family members whose cooperation made this work possible, Prof. Han G. Brunner for referring patients to this study; Sara McKay, Prof. R. Santer and Dr Tsiakas for clinical data; Dr Katalin Csiszar for a fibroblast cell line; Dr Robert P. Mecham and Dr Guojun Bu for antibodies; Dr Takahisa Kanekiyo for advice on immunostaining; the Facility for Electron Microscopy Research (FEMR) at McGill University and the EM facility of the Anatomy Department of the Charité for ultrastructural analysis.

Conflict of Interest statement. None declared.

FUNDING

This study was supported by the National Institutes of Health (HL084922 to Z.U.), by the Washington University Friedman Center for Aging (to Z.U.), the European Commission (LSHM-CT2005-512131, Euroglycanet to R.A.W.) and the Canadian Institutes of Health Research (MOP-86713 to E.C.D.). E.C.D is a Canada Research Chair.

REFERENCES

1. Das, S., Levinson, B., Vulpe, C., Whitney, S., Gitschier, J. and Packman, S. (1995) Similar splicing mutations of the Menkes/mottled copper-transporting ATPase gene in occipital horn syndrome and the blotchy mouse. *Am. J. Hum. Genet.*, **56**, 570–576.
2. Graul-Neumann, L.M., Hausser, I., Essayie, M., Rauch, A. and Kraus, C. (2008) Highly variable cutis laxa resulting from a dominant splicing mutation of the elastin gene. *Am. J. Med. Genet. A*, **146**, 977–983.
3. Rodriguez-Revenga, L., Iranzo, P., Badenas, C., Puig, S., Carrio, A. and Mila, M. (2004) A novel elastin gene mutation resulting in an autosomal dominant form of cutis laxa. *Arch. Dermatol.*, **140**, 1135–1139.
4. Szabo, Z., Crepeau, M.W., Mitchell, A.L., Stephan, M.J., Puntel, R.A., Loke, K.Y., Kirk, R.C. and Urban, Z. (2006) Aortic aneurysmal disease and cutis laxa caused by defects in the elastin gene. *J. Med. Genet.*, **43**, 255–258.
5. Tassabehji, M., Metcalfe, K., Hurst, J., Ashcroft, G.S., Kielty, C., Wilmot, C., Donnai, D., Read, A.P. and Jones, C.J. (1998) An elastin gene mutation producing abnormal tropoelastin and abnormal elastic fibres in a patient with autosomal dominant cutis laxa. *Hum. Mol. Genet.*, **7**, 1021–1028.
6. Urban, Z., Gao, J., Pope, F.M. and Davis, E.C. (2005) Autosomal dominant cutis laxa with severe lung disease: synthesis and matrix deposition of mutant tropoelastin. *J. Invest. Dermatol.*, **124**, 1193–1199.
7. Zhang, M.C., He, L., Giro, M., Yong, S.L., Tiller, G.E. and Davidson, J.M. (1999) Cutis laxa arising from frameshift mutations in exon 30 of the elastin gene (ELN). *J. Biol. Chem.*, **274**, 981–986.
8. Claus, S., Fischer, J., Megarbane, H., Megarbane, A., Jobard, F., Debret, R., Peyrol, S., Saker, S., Devillers, M., Sommer, P. *et al.* (2008) A p.C217R mutation in fibulin-5 from cutis laxa patients is associated with incomplete extracellular matrix formation in a skin equivalent model. *J. Invest. Dermatol.*, **128**, 1442–1450.
9. Loeys, B., Van Maldergem, L., Mortier, G., Coucke, P., Gerniers, S., Naeyaert, J.M. and De Paepe, A. (2002) Homozygosity for a missense mutation in fibulin-5 (FBLN5) results in a severe form of cutis laxa. *Hum. Mol. Genet.*, **11**, 2113–2118.
10. Dasouki, M., Markova, D., Garola, R., Sasaki, T., Charbonneau, N.L., Sakai, L.Y. and Chu, M.L. (2007) Compound heterozygous mutations in fibulin-4 causing neonatal lethal pulmonary artery occlusion, aortic

aneurysm, arachnodactyly, and mild cutis laxa. *Am. J. Med. Genet. A*, **143**, 2635–2641.
11. Hucthagowder, V., Sausgruber, N., Kim, K.H., Angle, B., Marmorstein, L.Y. and Urban, Z. (2006) Fibulin-4: a novel gene for an autosomal recessive cutis laxa syndrome. *Am. J. Hum. Genet.*, **78**, 1075–1080.
12. Morava, E., Lefeber, D.J., Urban, Z., de Meirleir, L., Meinecke, P., Gillessen Kaesbach, G., Sykut-Cegielska, J., Adamowicz, M., Salafsky, I., Ranells, J. *et al.* (2008) Defining the phenotype in an autosomal recessive cutis laxa syndrome with a combined congenital defect of glycosylation. *Eur. J. Hum. Genet.*, **16**, 28–35.
13. Freeze, H.H. (2006) Genetic defects in the human glycome. *Nat. Rev. Genet.*, **7**, 537–551.
14. Foulquier, F., Ungar, D., Reynders, E., Zeevaert, R., Mills, P., Garcia-Silva, M.T., Briones, P., Winchester, B., Morelle, W., Krieger, M. *et al.* (2007) A new inborn error of glycosylation due to a Cog8 deficiency reveals a critical role for the Cog1–Cog8 interaction in COG complex formation. *Hum. Mol. Genet.*, **16**, 717–730.
15. Foulquier, F., Vasile, E., Schollen, E., Callewaert, N., Raemaekers, T., Quelhas, D., Jaeken, J., Mills, P., Winchester, B., Krieger, M. *et al.* (2006) Conserved oligomeric Golgi complex subunit 1 deficiency reveals a previously uncharacterized congenital disorder of glycosylation type II. *Proc. Natl Acad. Sci. USA*, **103**, 3764–3769.
16. Wu, X., Steet, R.A., Bohorov, O., Bakker, J., Newell, J., Krieger, M., Spaapen, L., Kornfeld, S. and Freeze, H.H. (2004) Mutation of the COG complex subunit gene COG7 causes a lethal congenital disorder. *Nat. Med.*, **10**, 518–523.
17. Morava, E., Wopereis, S., Coucke, P., Gillessen-Kaesbach, G., Voit, T., Smeitink, J., Wevers, R. and Grunewald, S. (2005) Defective protein glycosylation in patients with cutis laxa syndrome. *Eur. J. Hum. Genet.*, **13**, 414–421.
18. Kornak, U., Reynders, E., Dimopoulou, A., van Reeuwijk, J., Fischer, B., Rajab, A., Budde, B., Nurnberg, P., Foulquier, F., Lefeber, D. *et al.* (2008) Impaired glycosylation and cutis laxa caused by mutations in the vesicular H^+-ATPase subunit ATP6V0A2. *Nat. Genet.*, **40**, 32–34.
19. Van Maldergem, L., Yuksel-Apak, M., Kayserili, H., Seemanova, E., Giurgea, S., Basel-Vanagaite, L., Leao-Teles, E., Vigneron, J., Foulon, M., Greally, M. *et al.* (2008) Cobblestone-like brain dysgenesis and altered glycosylation in congenital cutis laxa, Debre type. *Neurology*, **71**, 1602–1608.
20. Peralvarez-Marin, A., Lorenz-Fonfria, V.A., Simon-Vazquez, R., Gomariz, M., Meseguer, I., Querol, E. and Padros, E. (2008) Influence of proline on the thermostability of the active site and membrane arrangement of transmembrane proteins. *Biophys. J.*, **95**, 4384–4395.
21. Milewicz, D.M., Urban, Z. and Boyd, C. (2000) Genetic disorders of the elastic fiber system. *Matrix Biol.*, **19**, 471–480.
22. Kielty, C.M. (2006) Elastic fibres in health and disease. *Expert Rev. Mol. Med.*, **8**, 1–23.
23. Kozel, B.A., Rongish, B.J., Czirok, A., Zach, J., Little, C.D., Davis, E.C., Knutsen, R.H., Wagenseil, J.E., Levy, M.A. and Mecham, R.P. (2006) Elastic fiber formation: a dynamic view of extracellular matrix assembly using timer reporters. *J. Cell. Physiol.*, **207**, 87–96.
24. Davis, E.C. and Mecham, R.P. (1998) Intracellular trafficking of tropoelastin. *Matrix Biol.*, **17**, 245–254.
25. Davis, E.C., Broekelmann, T.J., Ozawa, Y. and Mecham, R.P. (1998) Identification of tropoelastin as a ligand for the 65-kD FK506-binding protein, FKBP65, in the secretory pathway. *J. Cell. Biol.*, **140**, 295–303.
26. Urban, Z., Riazi, S., Seidl, T.L., Katahira, J., Smoot, L.B., Chitayat, D., Boyd, C.D. and Hinek, A. (2002) Connection between elastin haploinsufficiency and increased cell proliferation in patients with supravalvular aortic stenosis and Williams–Beuren syndrome. *Am. J. Hum. Genet.*, **71**, 30–44.
27. Madsen, E.C. and Gitlin, J.D. (2008) Zebrafish mutants calamity and catastrophe define critical pathways of gene–nutrient interactions in developmental copper metabolism. *PLoS Genet.*, **4**, e1000261.
28. Dettmer, J., Hong-Hermesdorf, A., Stierhof, Y.D. and Schumacher, K. (2006) Vacuolar H^+-ATPase activity is required for endocytic and secretory trafficking in *Arabidopsis*. *Plant Cell*, **18**, 715–730.
29. Taupenot, L., Harper, K.L. and O'Connor, D.T. (2005) Role of H^+-ATPase-mediated acidification in sorting and release of the regulated secretory protein chromogranin A: evidence for a vesiculogenic function. *J. Biol. Chem.*, **280**, 3885–3897.
30. Tawfeek, H.A. and Abou-Samra, A.B. (2004) Important role for the V-type H(+)-ATPase and the Golgi apparatus in the recycling of PTH/PTHrP receptor. *Am. J. Physiol. Endocrinol. Metab.*, **286**, E704–E710.
31. Kinsey, R., Williamson, M.R., Chaudhry, S., Mellody, K.T., McGovern, A., Takahashi, S., Shuttleworth, C.A. and Kielty, C.M. (2008) Fibrillin-1 microfibril deposition is dependent on fibronectin assembly. *J. Cell. Sci.*, **121**, 2696–2704.
32. Sabatier, L., Chen, D., Fagotto-Kaufmann, C., Hubmacher, D., McKee, M.D., Annis, D.S., Mosher, D.F. and Reinhardt, D.P. (2009) Fibrillin assembly requires fibronectin. *Mol. Biol. Cell*, **20**, 846–858.
33. Gansner, J.M., Mendelsohn, B.A., Hultman, K.A., Johnson, S.L. and Gitlin, J.D. (2007) Essential role of lysyl oxidases in notochord development. *Dev. Biol.*, **307**, 202–213.
34. Vrhovski, B., Jensen, S. and Weiss, A.S. (1997) Coacervation characteristics of recombinant human tropoelastin. *Eur. J. Biochem.*, **250**, 92–98.
35. Zeuzem, S., Feick, P., Zimmermann, P., Haase, W., Kahn, R.A. and Schulz, I. (1992) Intravesicular acidification correlates with binding of ADP-ribosylation factor to microsomal membranes. *Proc. Natl Acad. Sci. USA*, **89**, 6619–6623.
36. Hinek, A., Pshezhetsky, A.V., von Itzstein, M. and Starcher, B. (2006) Lysosomal sialidase (neuraminidase-1) is targeted to the cell surface in a multiprotein complex that facilitates elastic fiber assembly. *J. Biol. Chem.*, **281**, 3698–3710.
37. Starcher, B., d'Azzo, A., Keller, P.W., Rao, G.K., Nadarajah, D. and Hinek, A. (2008) Neuraminidase-1 is required for the normal assembly of elastic fibers. *Am. J. Physiol. Lung Cell. Mol. Physiol.*, **295**, L637–L647.
38. Herrmann, B.G. and Frischauf, A.M. (1987) Isolation of genomic DNA. *Methods Enzymol.*, **152**, 180–183.
39. Wopereis, S., Morava, E., Grunewald, S., Adamowicz, M., Huijben, K.M., Lefeber, D.J. and Wevers, R.A. (2005) Patients with unsolved congenital disorders of glycosylation type II can be subdivided in six distinct biochemical groups. *Glycobiology*, **15**, 1312–1319.
40. Davis, E.C. (1993) Smooth muscle cell to elastic lamina connections in developing mouse aorta. Role in aortic medial organization. *Lab. Invest.*, **68**, 89–99.
41. Palamakumbura, A.H. and Trackman, P.C. (2002) A fluorometric assay for detection of lysyl oxidase enzyme activity in biological samples. *Anal. Biochem.*, **300**, 245–251.
42. Hinek, A. and Rabinovitch, M. (1993) The ductus arteriosus migratory smooth muscle cell phenotype processes tropoelastin to a 52-kDa product associated with impaired assembly of elastic laminae. *J. Biol. Chem.*, **268**, 1405–1413.